[5] Vimy MJ, Lorscheider FL. Intra-oral air mercury released from dental amalgam. J Dent Res 1985;64:1069–71.
[6] Vimy MJ, Lorscheider FL. Serial measurements of intra-oral air mercury: estimation of daily dose from dental amalgam. J Dent Res 1985;64:1072–5.
[7] Langworth S, Köhlbeck KG, Åkesson A. Mercury exposure from dental fillings. II. Release and absorption. Swed Dent J 1988;12:71–2.
[8] Berglund A, Pøhl L, Olsson S, Bergman M. Determination of the rate of release of intra-oral mercury vapor from amalgam. J Dent Res 1988;67:1235–42.
[9] Berglund A. Estimation by a 24 h study of the daily dose of intra-oral mercury vapor inhaled after release from dental amalgam. J Dent Res 1990;69:1646–51.
[10] Marek M. The release of mercury from dental amalgam: the mechanism and in-vitro testing. J Dent Res 1990;69:1167–74.
[11] Engle JH, Ferracane JL, Wichmann J, Okabe T. Quantitation of total mercury vapor released during dental procedures. Dent Mater 1992;8: 176–80.
[12] Berglund A, Molin M. Mercury vapor release from dental amalgam in patients with symptoms allegedly caused by amalgam fillings. Eur J Oral Sci 1996;104:56–63.
[13] Berglund A, Molin M. Mercury levels in plasma and urine after removal of all amalgam restorations: the effect of using rubber dams. Dent Mater 1997;13:297–304.
[14] Neme AL, Wagner WC, O'Brien WJ. Effects of palladium addition on emission of mercury vapor from dental amalgam. Dent Mater 1999; 15:382–9.
[15] Hanawa T, Takahashi H, Ota M, Pinizzotto RF, Ferracane JL, Okabe T. Surface characterization of amalgams using X-ray photoelectron spectroscopy. J Dent Res 1987;66:1470–8.
[16] Hanawa T, Gnade BE, Ferracane JL, Okabe T, Watari F. Compositions of surface layers formed on amalgams in air, water and saline. Dent Mater J 1993;12:118–26.
[17] Nakajima H, Akaiwa Y, Hashimoto H, Ferracane JL, Okabe T. Surface characterization of amalgam made with Hg–In liquid alloy. J Dent Res 1997;74:1414–7.
[18] McDermott AJ, Kothari S, Short RD, Van Noort R, Alexander MR. Surface chemistry of a high-copper dental amalgam. J Dent Res 1998; 77:1999–2004.
[19] Moulder JF, Stickle WF, Sobol PE, Bomben KD. Handbook of X-ray photoelectron spectroscopy. Eden Prairie: Physical Electronics Inc; 1992.
[20] Turkdogan ET. Physical chemistry of high temperature technology. New York: Academic Press; 1980.
[21] Mallard WG, Linstrom PJ, editors. NIST chemistry webbook. NIST standatd reference database number 69, Gaithersburg MD: National Institute of Standards and Technology; 2000. http://webbook.nist.gov
[22] Weast RC, editor. Handbook of chemistry and physics, 69th ed. Boca Raton, FL: CRC Press; 1989. p. F-52.
[23] Weast RC, editor. Handbook of chemistry and physics, 69th ed. Boca Raton, FL: CRC Press; 1989. p. E-147–9.
[24] Ferracane JL, Adey JD, Nakajima H, Okabe T. Mercury vapor from amalgams with varied alloy compositions. J Dent Res 1995;74: 1414–7.
[25] Okabe T, Yamashita T, Nakajima H, Berglund A, Zhao L, Guo I, Ferracane JL. Reduced mercury vapor release from dental amalgams prepared with binary Hg–In liquid alloys. J Dent Res 1994;73: 1711–6.

Available online at www.sciencedirect.com
SCIENCE DIRECT®
Composites Science and Technology 64 (2004) 893–908
COMPOSITES SCIENCE AND TECHNOLOGY
www.elsevier.com/locate/compscitech

Biocompatibility of materials and development to functionally graded implant for bio-medical application

Fumio Watari[a,*], Atsuro Yokoyama[a], Mamoru Omori[b], Toshio Hirai[c], Hideomi Kondo[a], Motohiro Uo[a], Takao Kawasaki[a]

[a] *Hokkaido University Graduate School of Dental Medicine, Sapporo 060-8586, Japan*
[b] *Institute for Materials Research, Tohoku University, Sendai 980-8577, Japan*
[c] *Japan Fine Ceramics Center, Mutuno 2-4-1, Atsuta, Nagoya 456-8587, Japan*

Abstract

Functionally graded materials (FGM) were fabricated for bio-medical application, especially for implant application, and the effect of gradient structure was evaluated. The titanium/hydroxyapatite (Ti/HAP) and other FGM implants with the concentration changed gradually in the longitudinal direction of cylindrical shape were fabricated by powder metallurgy to optimize both mechanical properties and biocompatibilities or change bioreactivity in each region. Concentration gradient was formed either by sedimentation in solvent liquid or by packing dry powders into mold, followed by compressing and sintering. Electric furnace heating, high frequency induction heating and spark plasma sintering (SPS) methods were used for sintering. SPS could make the stable Ti/HAP FGM. The Brinell hardness decreased gradually from Ti part to HAP part, which contributes for stress relaxation in the implanted region of bone. Tissue response and osteogenesis in animal implantation tests were evaluated from histological observation by optical microscopy and from elemental mapping by EPMA and XSAM (X-ray scanning analytical microscope). Maturation of bone is more advanced in the HAP rich region. The gradient functions in both mechanical properties and biochemical affinity to osteogenesis contribute to the efficient biocompatibility. These results demonstrated that the tissue reaction occurred gradiently in response to the graded structure of FGM, which implies the possibility to control the tissue response through the gradient function of FGM.

Keywords: A. Metal-matrix composites (NMCs); B. Mechanical properties; Biocompatibility; D. Electron microprobe analysis; E. Sintering

1. Introduction

For implants the materials need to satisfy the all-round properties of biocompatibility, strength and corrosion resistance. Titanium (Ti) is one of the best biocompatible metals and used most widely as implant [1]. Hydroxyapatite (HAP), main component of bone and teeth, has bioactive properties for new bone formation [2–4]. Glass [5–7] ia also one of the materials for bio-medical use.

Implant may be classified to "implant" as artificial bone for medical use and "dental implant" as artificial tooth for dental use. The specified properties are slightly different depending on their use. The implants in orthopaedics are used mostly as structurally enforced artificial bone which is inserted inside the corpus. Medical implants lay more weight on strength, toughness, torque in mechanical properties and the specific problem of tribology and abrasion resistance in artificial joint. Dental implant is usually much smaller and used to reconstruct the masticatory function, when tooth root is completely lost or extracted. It is set in the jaw-bone in the manner to penetrate from the inside to the outside of the bone. The function is, therefore, quite different at the inside of bone, outside and at their boundary. In the inside of jaw bone, bone affinity and stress relaxation are important and in the outside of bone, that is, in oral cavity, the sufficient strength is necessary.

The current dental implants composed of a single material, sometimes with a coating layer, are, however, essentially uniform in composition and structure in the longitudinal direction. The conception of FGM (functionally graded materials) [8–18] may be suitable to apply for implant. In Fig. 1 the expected properties of functionally graded dental implant were shown. The

* Corresponding author. Tel.: +81-11-706-4253; fax: +81-11-706-4251.
E-mail address: watari@den.hokudai.ac.jp (F. Watari).

0266-3538/$ - see front matter © 2003 Elsevier Ltd. All rights reserved.
doi:10.1016/j.compscitech.2003.09.005

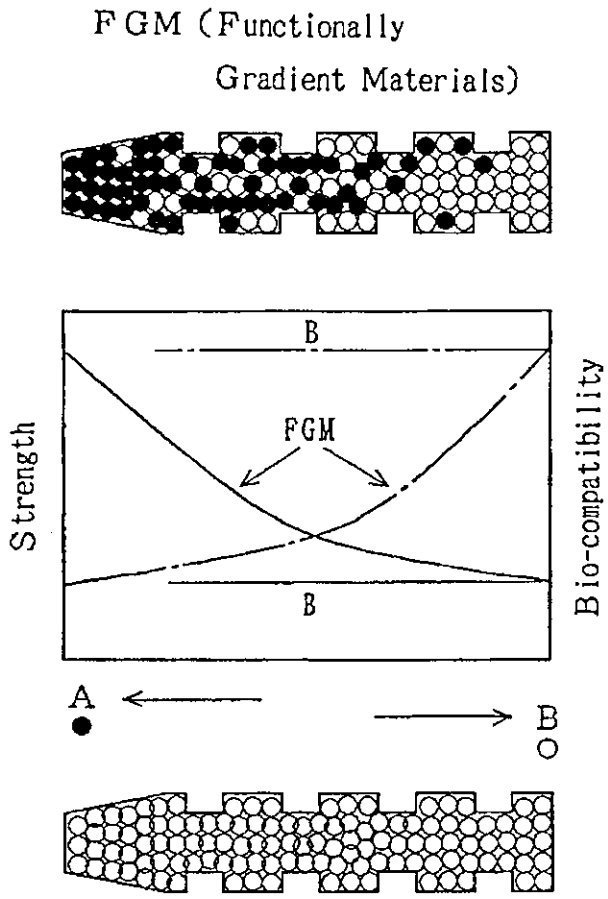

Fig. 1. Expected properties of functionally graded dental implant.

upper schema shows FGM implant and the lower shows the conventional uniform implant. The properties are shown in the middle. For the case of uniform implant the properties such as strength and biocompatibility are constant throughout the implant material. Meanwhile, the implant with the composition changed from the biocompatible metal, Ti, at one end (left in the figure), increasing the concentration of ceramics, HAP, toward 100% HAP at the other end (right), could control the functions of mechanical properties and biocompatibility, depending on the necessity of each part of implant, without the abrupt change due to the formation of discrete boundary. The implant was designed to provide more titanium for the upper part where occlusal force is directly applied and more apatite for the lower part which is implanted inside the jaw bone.

In the followings FGM implant with the structure changed, for example, from pure Ti at one end to Ti–20%HAP at the other end is expressed as Ti/20HAP and the specific region with the composition Ti–20%HAP [19] inside FGM is expressed as Ti-20HAP. Ti/HAP means Ti/100HAP and sometimes the general term for FGM composed of Ti and HAP.

The function of implant may develop further in future to control various bioresponse for the use as a small artificial internal organ. The biomaterials with the conception of FGM structure would serve most properly for this purpose. In the present study the animal implantation tests into both soft tissue and hard tissue were done to investigate the tissue reaction to the gradient composition of FGM structure.

The FGMs of Ti/20HAP [10–12], Ti/100HAP [16–18] and Ti/100Co [14,15] were fabricated by powder metallugy, using the different sintering methods. Ti/ZrO_2, Ti/SiO_2 [9,10], Ti (N)/HAP using surface-nitrided Ti which is expressed as Ti (N), and TiN/HAP were also made and investigated. The other pure metal implants of Ti, Zr, Hf, V, Nb, Ta, Re [1], Ni, Fe, Cu [20–22], Ag and alloys of Ni–Ti, SUS304, SUS316 [22], 12%Au–Ag–Pd–Cu dental alloys were also used for animal experiments for comparison. Laser welded biimplants, composed of combined equal length of metal cylinders, were also investigated in the system of Ti|Zr, Ti|Hf, T:|▽.

Another type of application, the polymer-ceramics FGM, was also done for dental core and post which is used for the case where most of tooth crown is lost and root is still remained [23,24]. Post is inserted in root canal after endodontic treatment and a crown made of metal or other materials is set on the core part to restore the mastication function. Photo-polymerization type composite resin with ceramics filler in polymer resin matrix was used as material. Functionally graded core and post was fabricated by laser lithography, one of the photo-curing type CAD/CAM systems, for stress relaxation at the tooth root by decreasing the filler content ratio from core part down to the apex of post.

In the present paper we focus the main attention on Ti/HAP FGM implant since this is the most interesting and promising for clinical application. This system is, however, not easy to fabricate since the optimum conditions of sintering for Ti and HAP is very different and the sintering condition for their mixture is obliged to make compromise. In the following some of the accomplishments are shown on fabrication, imaging as evaluation, mechanical properties, animal implantation tests and their problems of FGM as well as uniform metals, alloys and biimplants,

2. Experimental procedure

2.1. Implant materials

Table 1 summarizes the specimen preparation methods for uniform, biimplant and gradient implant specimens used in this study. FGM implants were prepared by powder metallurgy, changing gradually the concentration along the longitudinal direction either by dry method or wet method. In the dry method the mixed powders with the varying concentration of 99.98% Ti or Ti hydrate (Sumitomo Sitix) and HAP (Sumitomo Osaka Cement)

Table 1
Specimen preparation methods for uniform, biimplant and gradient implant specimens

Gradient Formation
Dry: Powder packing Wet: Sedimentation
Condensation + Sintering
CIP (Cold Isostatic Press: 400–1000 MPa) + EF (Electric Furnace heating: 1300 °C)
CIP (400 MPa) + HF (High Frequency Induction Heating: 1200 °C)
SPS (Spark plasma sintering: 20–80 MPa, 850 °C) LW (Laser Welding: Nd–YAG, pulse mode, for biimplant).

or 99% Co were packed into the mold. In the wet method [14], two kinds of Ti powders (<45 μm and <150 μm) and two kinds of HAP powders (<20 μm and 20–45 μm) were mixed and stirred in methanol. After the mixture was poured into the tube of 4 mm in an inner diameter and left for sedimentation, the supernatant was removed and dried at 40 °C.

Electric furnace heating [10–15], high frequency induction heating [9–12] and spark plasma sintering (SPS) methods [16–19] were used for sintering. In the electric furnace heating, powders were packed into the thermo-contractive tube with a 0.25 mm thickness. After the heat treatment of a tube at 60 °C, Ti/20HAP and Ti/Co were compressed by CIP (Cold Isostatic Press) at 800–1000 MPa. The implants of the miniature cylindrical shape 2×7 mm or 3×7 mm were then made by sintering in vacuum of 10^{-3} Pa at about 1300 °C for pure Ti, Ti/20HAP, Ti/100HAP FGMs and at 1100 °C for Ti/Co FGM.

In the high frequency induction heating, powders were packed into the thermo-contractive tube or silicone rubber impression mold with the shape of dental implant. After CIP the compacts were sintered at above 1300 °C in Ar gas atmosphere. Ti/20ZrO_2, Ti/20SiO_2 were also prepared.

For SPS (IZUMITECH) the mixed powders of Ti hydrate (SUMITOMO SITIX) and HAP were packed in graphite mold of 200×(7–14) mm with the gradient composition ranged from pure Ti to 100%HAP in the height direction and sintered at 850 °C under the pressure of 40 or 80 MPa. After sintering, the square rods of 1×1×(7–10) mm, 3×3×7 mm and 2×2×14 mm were cut out for animal implantation test, compression test and three point flexural test, respectively, and mechanically polished up to #2000 on the surface. The various FGM specimens were also prepared: Ti/50HAP, 20HAP/50HAP, 50HAP/80HAP, 20HAP/80HAP, 50HAP/100HAP, Ti (N)/HAP and TiN/HAP.

The uniform implants and biimplants were also prepared for comparison in animal experiments. For pure metal implant the wire of 10×10 mm of 99.9%Ti was used other than Ti rod prepared by powder metallurgy. The wire of 10×7 mm was used for 97%Hf, 99.9%Nb, 99.95%Ta, 99.97%Re and the square rod of 0.5×2×10 mm was used for 99.7%Ni. The alloys of Ni–Ti, SUS304, SUS316, 12%Au–Ag–Pd–Cu dental alloys were also used. Bi-implants were prepared by welding the equal length of metal cylinders for the system of Ti|Zr, Ti|Hf, Ti|V using the dental laser welder (TANAKA LaborLaser TLL7000PLUS).

2.2. Mechanical tests

Specimens prepared and evaluation methods used in this study are listed up in Tables 2 and 3, respectively. Brinell hardness was measured in each region inside the Ti/HAP FGM. Compression test was done with the specimens of 3×3×7 mm and the three point flexural test in gauge length 14 mm [6,7] was done with the specimens of 2×2×14 mm, using the universal testing machine (Instron 4204).

2.3. Animal implantation test

FGM implants as well as uniform implants and biimplants were inserted into hard tissue, bone marrow of femora of rats or tibia of rabbits, for 1–8 weeks and into subcutaneous soft tissue in the dorsal or ventral thoracic region for 1–2 weeks. Pure Ti was implanted in every case for comparison.

2.4. Observation and analysis

To observe the implant surface and mechanically polished cross section before implantation and to evaluate the tissue response and osteogenesis after implantation, the observation by optical microscopy (Olympus Vanox-S, Zeiss Axioskop 50), scanning electron microscopy (SEM/Hitachi S2380N, S4000), and elemental line analysis, mapping by EPMA (electron probe microanalysis/JEOL JXA8900) and XSAM (X-ray scanning analytical microscope/Horiba XGT2000V) [20–22] were performed. After the tissue blocks were fixed, they were dehydrated, embedded in resin or paraffin, sectioned to the thickness 100 μm in hard tissue and 5 μm in soft tissue, respectively, and stained. These specimens were served for histological observation by optical microscopy. The unstained, thick specimens with only one side polished were used for compositional image by SEM and elemental mapping by EPMA and XSAM. The spatial resolution of mapping is about 1 μm in higher magnification by EPMA and 100 μm by XSAM.

3. Results

Fig. 2 is the SEM image of the cross section of Ti/20HAP FGM implant around the region biased toward

Table 2
Prepared specimens

Materials	Preparation method	Ref.
Pure metals, alloys, composites (uniform composition)		
Ti, Zr, Hf, V, Nb, Ta, Re		[1]
Ti, Ni, Fe, Cu		[20,21]
Ti, Ni, Fe, Cu, TiNi, SUS304, SUS316		[22]
Ag, 12%Au–Ag–Pd–Cu		
Ti–HAP	SPS	[19]
Biimplant		
Ti|V, Ti|Zr, Ti|Hf	LW	
Functionally graded implant		
Ti/20HAP, Ti/Co	CIP + EF	[14,15]
Ti/20SiO_2, Ti/20ZrO_2, Ti/30HAP	CIP + HF	[9,10,12]
Ti/30HAP, Ti/50HAP, Ti/HAP (Ti/100HAP)	SPS	[16,17,18]
50HAP/100HAP, 70HAP/100HAP	SPS	
20HAP/50HAP, 50HAP/80HAP, 20HAP/80HAP	SPS	
TiN/HAP, Ti (N)/HAP	SPS	

Table 3
Evaluation methods for uniform, biimplant and gradient implant specimens

Imaging
Visual
OM (optical microscope)
Reflection
Transmission (histopathological observation of implanted tissue)
SEM (scanning electron microscope)
EPMA (electron probe microanalysis)
XSAM (X-ray scanning analytical microscope)
Spectroscopy
WDS (wavelength dispersive spectroscopy)-EPMA
EDS (energy dispersive spectroscopy)-XSAM
Raman spectroscopy
Mechanical test
H.. (Brinell hardness)
σ_c (compressive strength)–compression test
σ_c (flexural strength)-three point flexural test
Biocompatibility test
Implantation in hard tissue and in soft tissue of rat

Ti–20HAP in the right end. The implant has the miniature cylindrical shape of 20×7 mm. The distribution of HAP particles could be recognized inside the Ti matrix. Most of HAP particles are less than 100 μm and their density was increased toward the right.

Fig. 3 shows the Ti (a), P (b) and Ca (c) mapping images by XSAM of Ti/100HAP FGM prepared by sedimentation method. The content of Ti decreases toward the right end and that of Ca, component of HAP, decreases toward the left end. The contrast looks complementary for Ti and Ca. At each end the composition is nearly pure Ti and HAP. However, the changing manner of concentration in P mapping is not the same as that of Ca (Fig. 3b). In the direction from right to left P content was abruptly decreased to nearly null in the center-right, approximately quarter sized region of the whole length and reappeared with lower concentration in the left-half region.

Fig. 4 shows the Ti/HAP FGM after Brinell hardness test observed in profile imaging mode by reflection electrons in SEM. FGM was made by dry method with electric furnace sintering at 1300 °C. The size of round

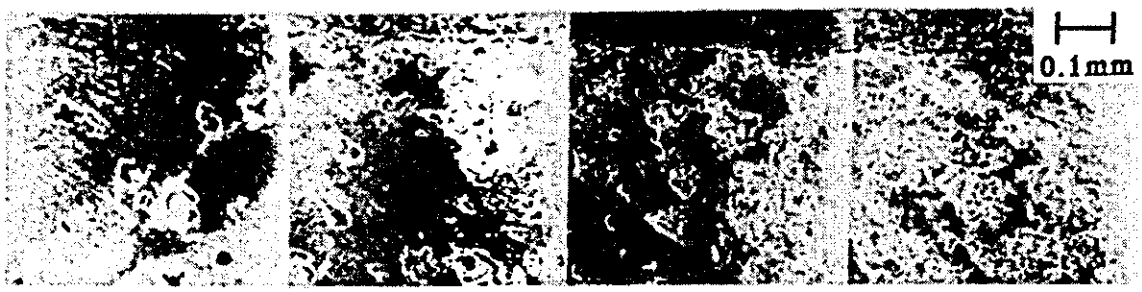

Fig. 2. SEM image of the cross section of Ti/20HAP FGM implant around the region biased toward Ti–20%HAP (right side).

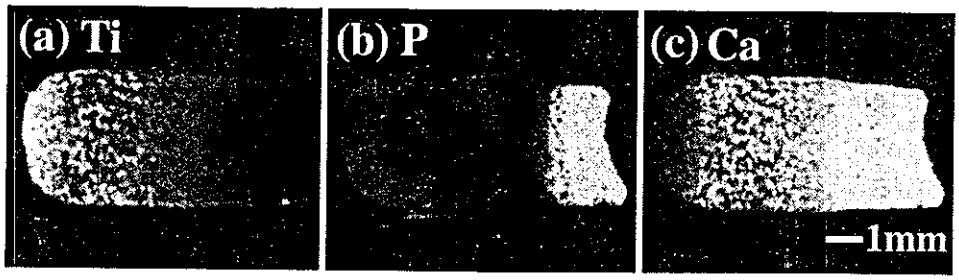

Fig. 3. XSAM elemental mapping of Ti/HAP FGM formed by sedimentation method. a:Ti, b:P, c:Ca.

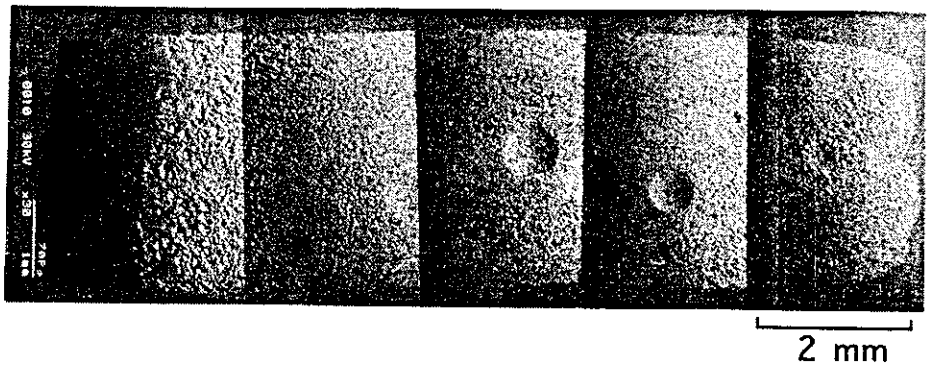

Fig. 4. Ti/HAP FGM after Brinell hardness test observed in profile imaging mode by reflection electrons in SEM where the size of round indentations made by testing in each region indicates the change of hardness.

indentations made by testing expresses the change of hardness from region to region.

Brinell hardness changed with HAP content in the Ti/HAP FGM corresponding to Fig. 4 is shown in Fig. 5a (dotted line). The hardness was about 70 in both Ti and HAP region, and low in the center region where Ti and HAP were mixed with comparable content. There occurred the delayed expansion, followed by spontaneous destruction, after 1 month in this specimen.

Fig. 6 shows the various FGM specimens composed of Ti and HAP, made by SPS method. In the right direction HAP content is increased. Fig. 6a is Ti/50HAP, b is 20HAP/50HAP, c is 50HAP/80HAP, d is 20HAP/80HAP and e is 50HAP/100HAP. Ti/100HAP made by SPS is shown later in Fig. 12a. All these specimens prepared by sintering at 850 °C under 80 MPa using SPS method are stable and endurable to the process of machining, animal implantation and evaluation process.

Fig. 5b (solid line) shows the change of Brinell hardness with HAP content in the Ti/100HAP FGM made by SPS corresponding to Fig. 12a. Ti/HAP FGM is composed of eleven layers with the composition difference by every 10%. Brinell hardness decreased from 61 in pure Ti to 15 in pure HAP, which is the different tendency from Fig. 5a.

The dependence of compression and flexural strength of Ti/HAP FGM on SPS pressure was investigated. For SPS pressure 40 and 80 MPa, compression strength increased increased from 47 to 88 MPa and flexural strength remarkably from 7 to 36 MPa. The fracture in flexural test occurred inside the single layer situated in the center for 80MPa as seen in Fig. 12a. For 40 MPa fracture occurred, deviated from center, in the weaker HAP-rich side and the value (7 MPa) is shown for reference.

Fig. 7 is the external appearance (left) and cross-section (right) of Ti/20HAP FGM dental implant. The upper part, which situates inside the mouth and needs the mechanical properties, is composed of pure Ti, while in the lower part, which situates inside the jaw bone, the content of HAP increases toward the lower up to 20% apatite in the end to provide more biocompatibility.

Fig. 8 shows the subcutaneous soft tissue of rat around Ni after 2 week implantation. Ni implant had been inserted in the hole situated in the center. Observation by optical microscopy (a) and Ca (b), Fe (c), Ni (d) mappings by XSAM were compared. The severe inflammation, hemorrhage and necrosis were induced around Ni implant (Fig. 8a). The inflammatory area observed by optical microscopy (Fig. 8a) corresponds well to the dissolved region of Ni revealed by Ni mapping of XSAM (Fig. 8d). The dissolved concentration of Ni was in the level of 100 ppm [22] and decreased as a function of distance from Ni surface. There was a good relation between the gradient concentration of dissolved Ni and the degree of degeneration of tissue. The region of hemorrhage which looks black in the optical microscopic image (Fig. 8a) corresponds well to the distribution of Fe in Fig. 8c which was contained in hemoglobin. It looks that there was the enrichment of Ca, surrounding Ni implant.

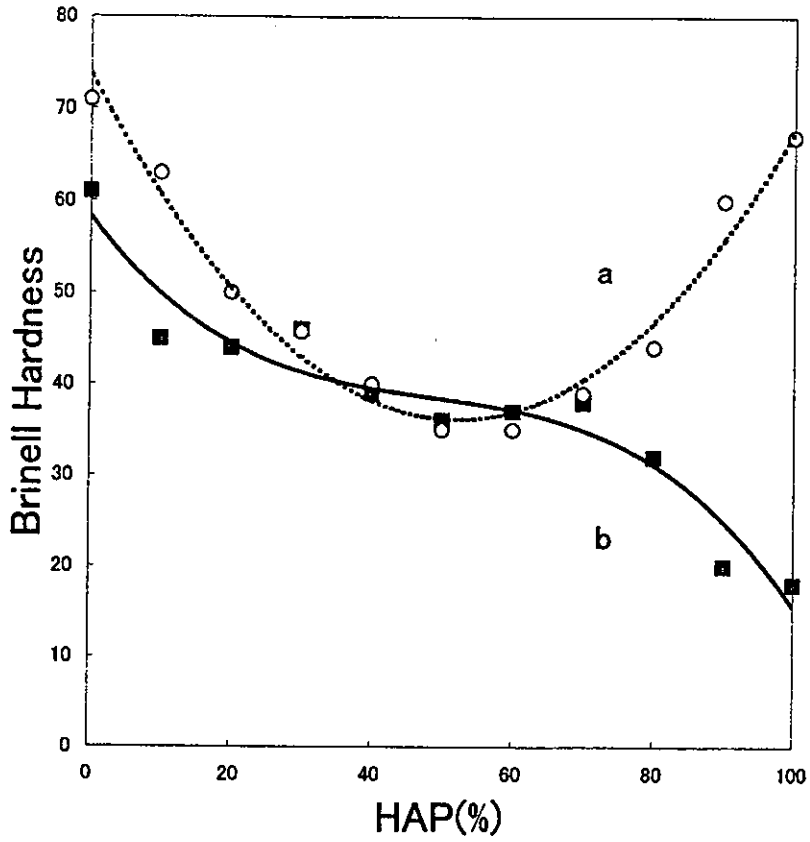

Fig. 5. Change of Brinell hardness with HAP content in Ti/HAP FGM; a is corresponding to FGM of Fig. 4, sintered by electric furnace heating at 1300 °C; b is corresponding to Fig. 12a, sintered by SPS at 850°C.

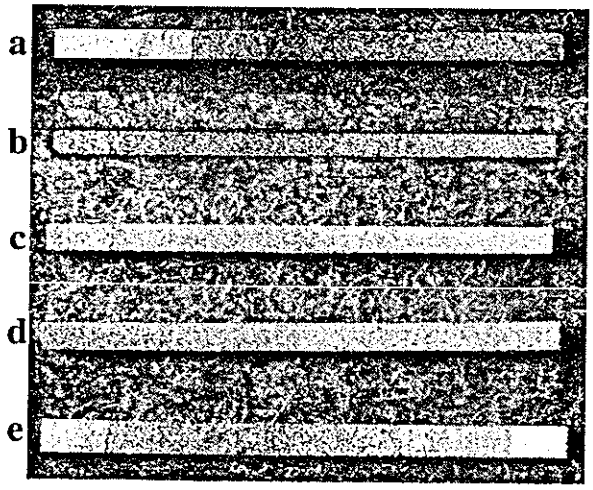

Fig. 6. Various FGM specimens composed of Ti and HAP, made by SPS method (right: HAP rich region): a: Ti/50HAP, b: 20HAP/50HAP, c: 50HAP/80HAP, d: 20HAP/80HAP, e: 50HAP/100HAP.

Fig. 9 shows the comparison of tissue reaction to Ni (a), Ti (b), Fe (c), Ag (d), NiTi (e) and SUS316 (e) after 1 week implantation in the dorsal thoracic region of rat. Implant had been situated in the upper space of each photograph. Fibrous connective tissue was formed around Ti, Fe and Ni–Ti, and under the forming process in Ag and SUS316, while necrosis occurred around Ni. In Ni the expansion of capillary vessels was observed and tissue was in necrosis and in degeneration in the distant region. Ti showed the formation of fibrous connective tissue surrounding implant from the earlier stage and the most sound reaction from histopathological view point. In Fe, tissue had little inflammation and the formation of fibrous connective tissue surrounding implant was observed at this stage. NiTi is similar to Ti. The well stained nuclei of fibroblasts were observed more inside the fibrous connective tissue than Ti, which suggests the slightly longer time would be needed to be in the same condition as pure Ti. In both Ag and SUS316 the formation of fibrous connective tissue was not completed yet and was in the process on the way. The comparison makes noticeable the difference of biocompatibility among these metals sensitively.

Fig. 10 shows the Ti/Co FGM specimen and its effect in the soft tissue after 2 week implantation in the subcutaneous tissue of dorsal part of rat. The left side in Fig. 10a is pure Ti and the right is pure Co. The concentration of Co increases from left to right along the longitudinal direction. Fig. 10c shows the histological observation of the fibrous connective tissue formed around implant. The implant which was removed from

Fig. 7. Ti/20HAP FGM dental implant. External appearance is shown in the left and cross-section in the right.

soft tissue had been situated in the upper side of the photograph Fig. 10c. The thickness of the fibrous connective layer was small in the pure Ti region in the left side and increased toward the right side as the concentration of Co increased along the longitudinal direction of FGM. In the right end the tissue was inflammatory and necrosis occurred in some parts.

The elemental mapping of S, P, Ca, Ti and Co was done for the specimen of Fig. 10 by XSAM. S, Ca and P whose concentration was low enough, of the order of 100ppm in soft tissue, were detected by XSAM and showed the distribution in the whole area of soft tissue. The Ti mapping showed no trace of Ti dissolution. The mapping of Co (Fig. 10b) revealed that the dissolution of Co into the surrounding soft tissue was prominent around the right part of implant. The changing concentration of dissolved Co along the implant toward the right is well coincided with the increase of thickness of tissue layer and the degree of inflammatory response in Fig. 10c.

The wires of Ti, Hf, Nb, Ta, Re implanted in rats showed no inflammatory reaction in soft tissue and in hard tissue. They have enough biocompatibility with a slight difference in new bone formation around implant [1].

Fig. 11 is the histological observation of bone formation and resorption around Ti|V biimplant inserted in the tibia of rabit for 4 weeks. In Ti part (a) new bone was formed directly contact to implant, while cortical bone looked absorbed in the part contacting to V and juvenile immature bone was formed with separation from V (b). Ca mapping by EPMA showed that the density of Ca in new bone around Ti is nearly the same as the cortical bone. On the other hand Ca enrichment was inferior in new bone formed around V. In the Ti|Zr and T|Hf biimplants new bone was formed directly contact to metal surface on both sides of biimplants and Ca enrichment was nearly equivalent to the cortical bone.

Fig. 12a shows the Ti/HAP functionally graded implant (left: Ti, right: HAP) made by SPS under the sintering pressure of 80 MPa after three point flexural test. The 11 layers with the composition difference by every 10% can be recognized. The fracture occurred inside the one layer in the center. Fig. 12b and c are the Ca and Ti mappings by EPMA for Ti/HAP FGM after 8 week insertion in the bone marrow of femora of rat. Ca as representative element of HAP is gradually increased in the longitudinal direction to the right inside the implant. Ca, also as representative element of bone, showed the new bone formed surrounding the implant. Lower-left region is cortical bone. Ti (Fig. 12c), inversely and complementarily to Ca, decreased to the right direction.

Fig. 13 is the histological image around the Ti side (a) and the HAP-rich side (b) in the Ti/HAP FGM implant (I) inserted in the bone marrow (BM) of femora of rat for 16 weeks. New bone (NB) was formed with the thicker but wavy external form, less contact to the implant surface, in the Ti rich region, while with the thin and smooth form, directly contact to the implant in the HAP rich region.

Fig. 14 is the enlargement of new bone formation around the HAP rich region (Ti–80HAP) of Ti/HAP FGM shown in Fig. 13. In Fig. 14 a is HAP matrix, b is Ti particles, c is new bone. Non-transparent Ti particles (b) are dispersed in the semi-transparent HAP matrix (a). Transparent new bone (c) is formed in direct contact on the surface of implant material. New bone

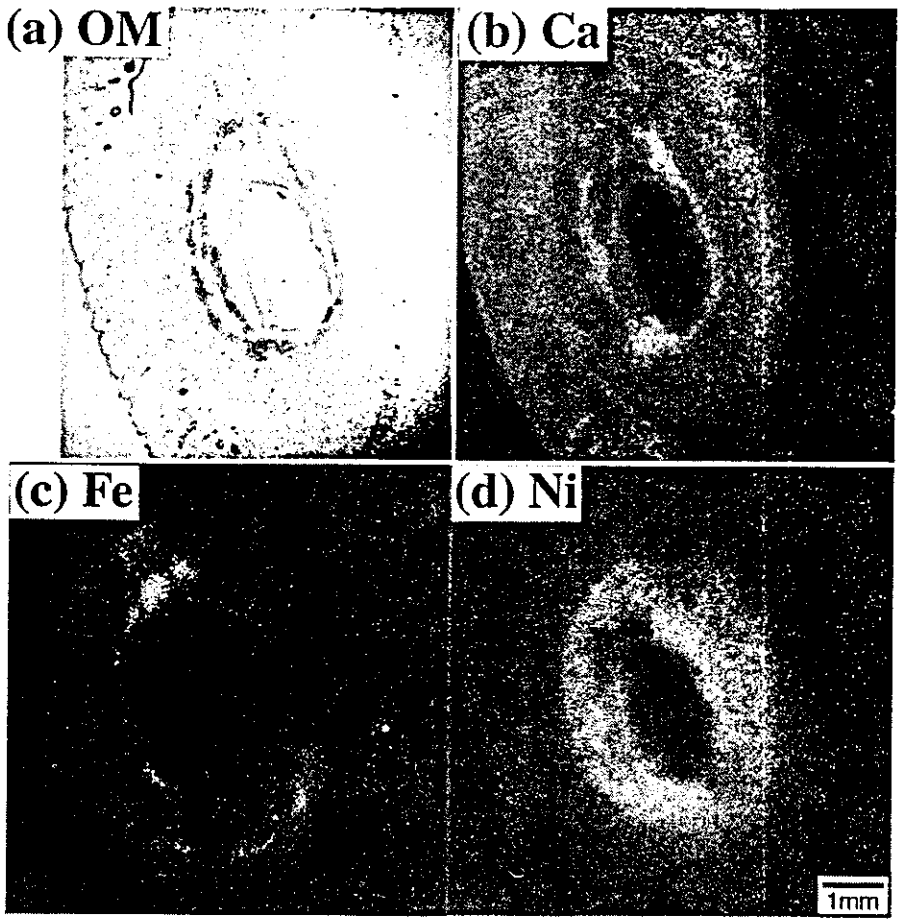

Fig. 8. Subcutaneous soft tissue of rat around Ni after 2 week implantation. Observation by optical microscopy (a) and Ca (b), Fe (c), Ni (d) mappings by XSAM.

showed the lamella structure as a result of bone remodeling, which is the feature of maturation of bone.

4. Discussion

4.1. Fabrication of FGM implant

Ti and HAP is a difficult combination to make FGM by powder metallurgy. The optimum sintering conditions are very different. HAP is stable in the oxidizing atmosphere, while Ti needs the vacuum or reducing atmosphere since Ti is easily oxidized. As sintering temperature HAP needs more than 1150 °C and Ti needs more than 1300 °C. HAP which contains OH^- and 3-PO4 becomes unstable in vacuum and decomposed under the coexistence with Ti particles. Dephosphoration occurs as one of the decomposition phenomena.

XSAM mapping of Ti/HAP FGM prepared by sedimentation method in Fig. 3 showed the gradual decrease of Ca toward the left end. However, the changing manner of concentration in P mapping is not the same as that of Ca (Fig. 3b). Both Ca and P are the main component elements of HAP, therefore both should show the similar concentration gradient. P content was, nevertheless, abruptly decreased to nearly null in approximately one quarter of the whole length to the left direction and reappeared with lower concentration in the center-left region. This suggests the decrease of P content, much lower than that expected from the nominal composition in HAP. Micro-area X-ray diffraction showed the formation of $CaTiO_3$ (Perovskite) in HAP-rich Ti mixed region. In the reducing atmosphere or vacuum at high temperature HAP is unstable when Ti is coexistent and dephosphoration might occur. In this sedimentation method to make the composition gradient, Ti particles sedimented faster at bottom side with its larger density and HAP particles sedimented more slowly due to smaller density. There is also a size distribution in Ti and HAP particles. The larger Ti particles sedimented faster and formed the bottom part, that is, the left end in Fig. 3. The finer Ti particles tended to sediment more slowly and exist more in the supernatant side, that is, HAP rich side in the right. Finer Ti

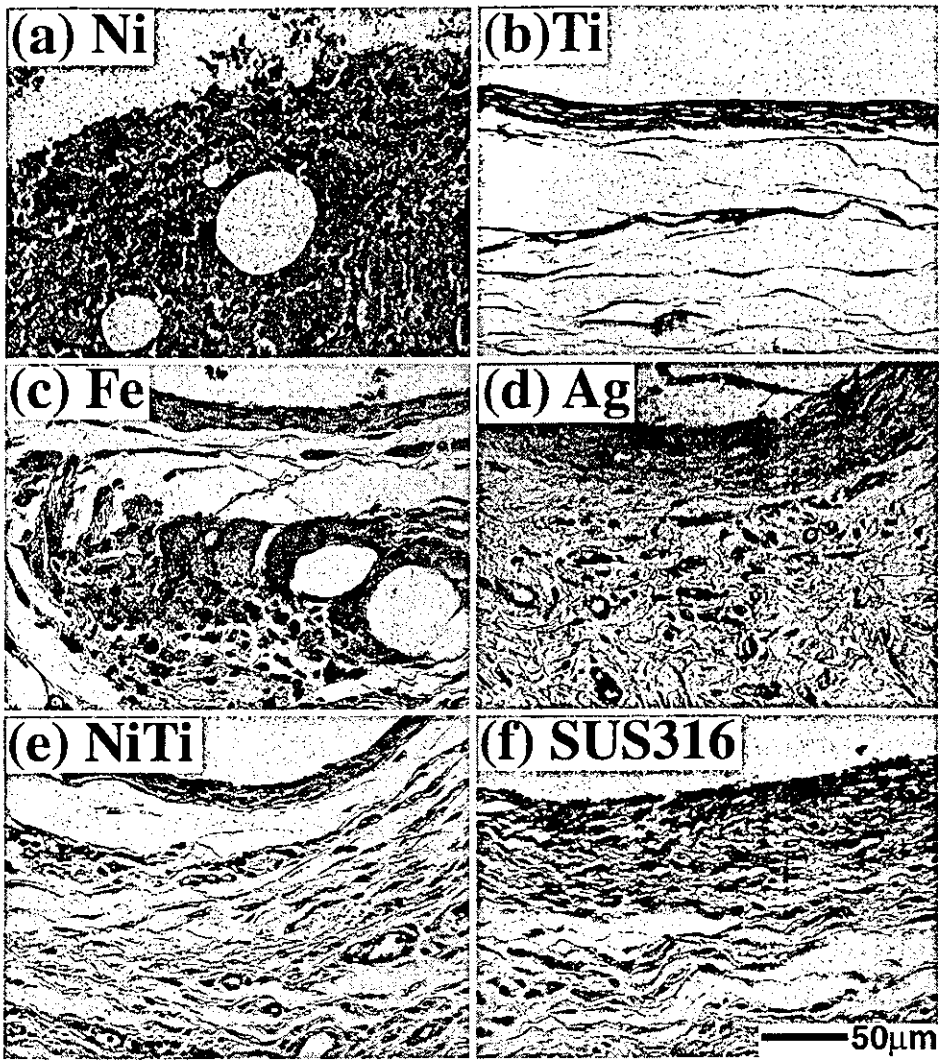

Fig. 9. Tissue reaction to Ni (a), Ti (b), Fe (c), Ag (d), NiTi (e) and SUS316 (e) after 1 week implantation in rat.

particles work more effectively to decompose HAP in vaccum and make dephosphoration. This leads to the formation of $CaTiO_3$ where P is not included as component, which explains well the XSAM mapping of Fig. 3.

Brinell hardness changed inside the Ti/HAP FGM in Fig. 4 showed that the hardness was low in the center region where Ti and HAP were mixed with comparable content (Fig. 5a). This is partly due to the decrease of compressing effect in the center of compact, remote from surface, by friction between particles in the CIP compacting process [25]. Another reason may be due to the decomposition occurred in the mixed region of Ti and HAP, since more than 1150 °C is necessary for sintering of Ti and HAP in the electric furnace method. The delayed expansion occurred and lead to autodestruction approximately in a month after fabrication due to the decomposition of HAP and the residual stress. To prevent this phenomenon, improvements in both materials and methods have been done.

Although the same phenomena occurred in SPS method, we could successfully prepare the Ti/HAP FGM by removal of Ti finer particles smaller than 1 μm using the sedimentation method for elimination and by lowering the sintering temperature to 850 °C.

4.1.1. Starting materials

HAP as prepared by wet methods are deviated from stoichiometry and generally unstable under heat treatments. HAP sintered at more than 1150 °C in air shows the peak due to stretching mode of OH.. group in FT-IR and Raman spectroscopy [18], which does not appear or is very small in HAP as prepared in wet method. Sintered HAP is close to stoichiometric and more stable to heat treatment. The HAP frit prepared by pulferization after sintered was used as starting material for HAP.

For Ti the particles of Ti hydrate instead of pure Ti seemed more favorable for sintering. Ti fine particles less than 1 μm causes more decomposition of HAP. The

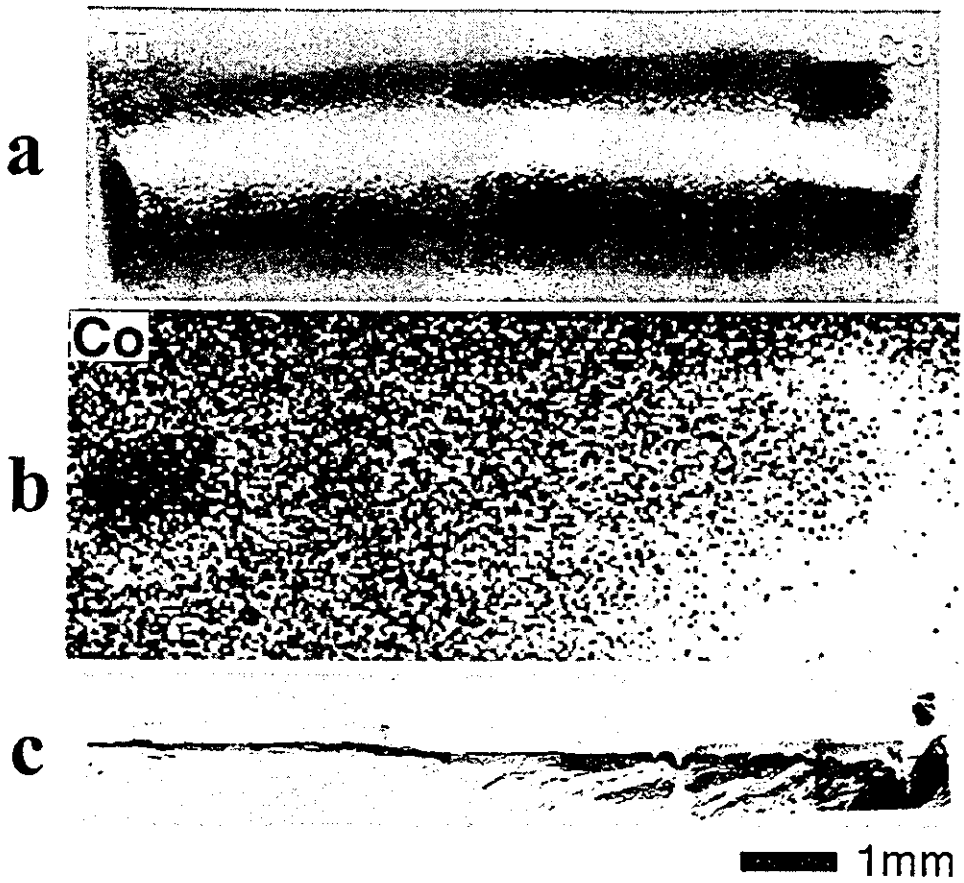

Fig. 10. Correlation of Ti/Co FGM (a), dissolution area of Co (b) and surrounding tissue reaction (c) after 2 week implantation in subcutaneous tissue of rat.

325 mesh pass Ti powders were sedimented and finer particles smaller than 1 μm was removed.

4.1.2. Sintering methods

After compacting by CIP, sintering was done in vacuum or inert gas atmosphere (Ar). As method for sintering (1) electric furnace heating, (2) high frequency induction heating, (3) spark plasma sintering (SPS) were used.

(1) The most common method for sintering is electric furnace heating. CIP compacting with 400 MPa was not enough for sintering of Ti. The 700–1000 MPa CIP pressure was preferable. Heating at more than 1300 °C was necessary for sintering of Ti in vacuum. Under this condition HAP became unstable and decomposition began to occur. Heating is done in the mode from the outside of specimens. Expansion and contraction initiates at surface during heating and cooling process. Internal stress tends to be induced more, especially in the cooling process, which is another cause to produce the delayed fracture with higher probability. The product of FGM up to 30HAP could be stably formed, but Ti/100HAP was resulted in autodestruction.

(2) High frequency induction heating can heat to high temperature enough for sintering of Ti and HAP easily. Sintering can be finished quickly. Ti or other metal particles are heated by itself from the inside, therefore the internal stress due to thermal expansion and contraction may be relatively less produced and it is favorable for sintering of Ti whose surface is covered with strong oxide layer. In principle only metals are heated and heat is not generated in ceramics. This may help to make the decomposition of HAP relatively less and could make the stable FGM. However HAP content is limited up to 30 wt.% in our experience and up to 50 wt.% if Ti wire is inserted in the center core of 2–3 mm. cylinder. It was not possible to fabricate FGM from pure Ti to 100%HAP.

(3) SPS can heat both metal and ceramics, even polymers. One may also expect further effects such as spark plasma between particles. This may break the surface oxide layer of Ti, enhance sintering, and lower the sintering temperature and the decomposition of HAP. The stable Ti/HAP FGM endurable to machining and animal implantation test followed by specimen prepara-

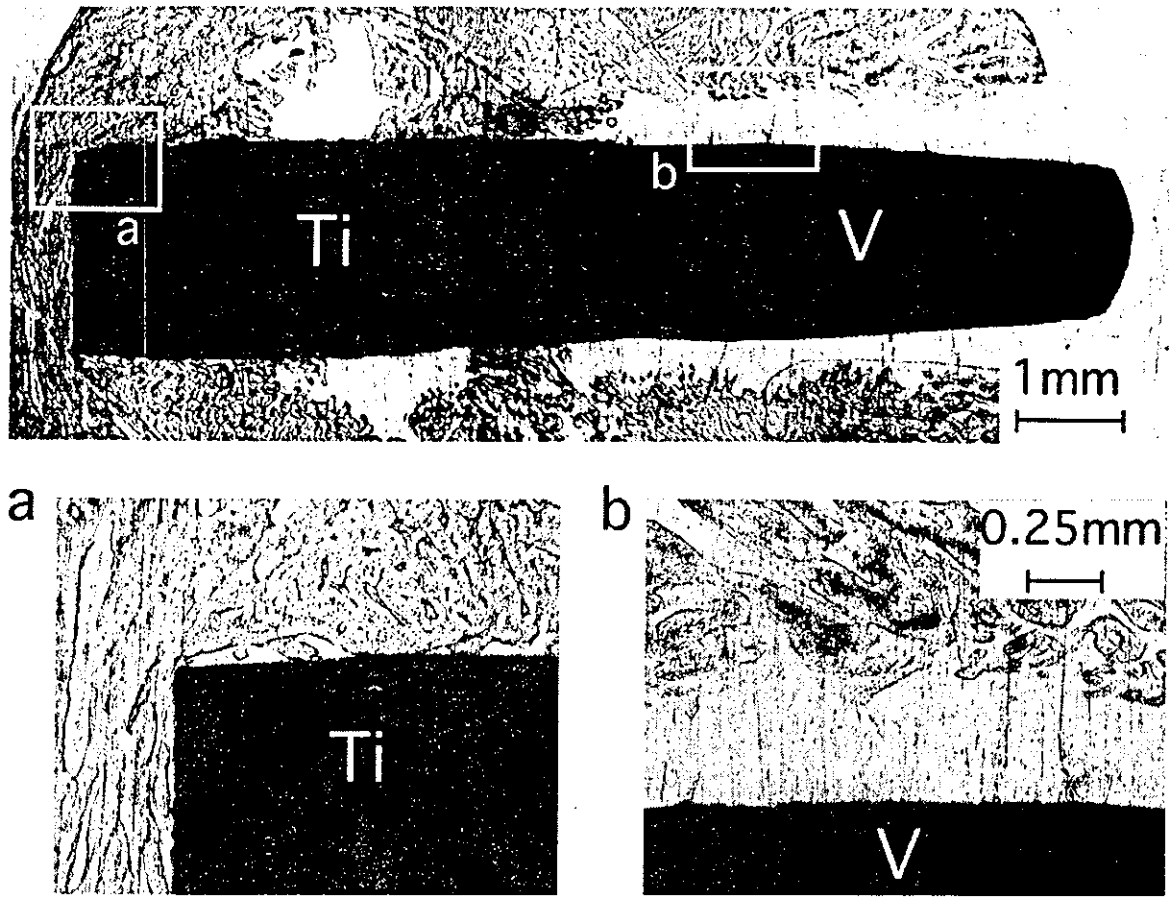

Fig. 11. Histological observation of bone formation and resorption around Ti|V biimplant inserted in tibia of rabit for 4 weeks. New bone was formed directly contact to Ti (a), while juvenile immature bone was formed apart from V (b).

tion including diamond saw cutting and polishing could be realized by sintering at 850 °C much lower than 1300 °C in the conventional sintering method. Raman spectra from 100%HAP area showed the prominent peak of OH. around 3550 cm^{-1}, which does not necessarily appear in many hydroxyapatites and implies the excellent crystallization [18].

However this is still the compromise to sacrifice to some extent the full sintering. To enhance the sintering effect the sintering pressure was increased from 20 to 40 MPa and further to 80 MPa. The attainment of higher SPS pressure is controlled by the strength of mold material rather than the pressing capacity of SPS instrument. At higher than 650 °C the creep deformation occurs in the hard metal WC–Co alloy. By use of high strength graphite 80 MPa was possible to impose instead of 20 MPa using the ordinary graphite [17,18].

4.2. Imaging of FGM structure

Various imaging methods [26–30] were applied to observe and evaluate the functionally graded structure and tissue reaction around implant inserted in animal experiment [13,15]. After the external appearance was observed either with the naked eye or by optical microscopy, X-ray tranmission image [11] was taken. The cross section was investigated by secondary electron image and compositional image [1,11,30] using the reflection electrons in SEM. The FGM specimens intentionally without the deposition of metal coating layer on surface were also used in the observation of the usual seconary electron image in SEM. HAP is electronically nonconductive and exhibits the excess brightness by electron charging effect in SEM observation, which makes easier recognition of HAP particles in the Ti matrix [12]. Line analysis and elemental mapping was done by EPMA and XSAM [11–13,20–22].

The optical image is based on the reflection and scattering of light, dependent on surface morphology. X-ray transmission and reflection electron images are based on the absorbance and reflectivity which are dependent on atomic number. Line analysis and mapping is based on characteristic X-ray emission. All these methods were used to confirm the gradient structure.

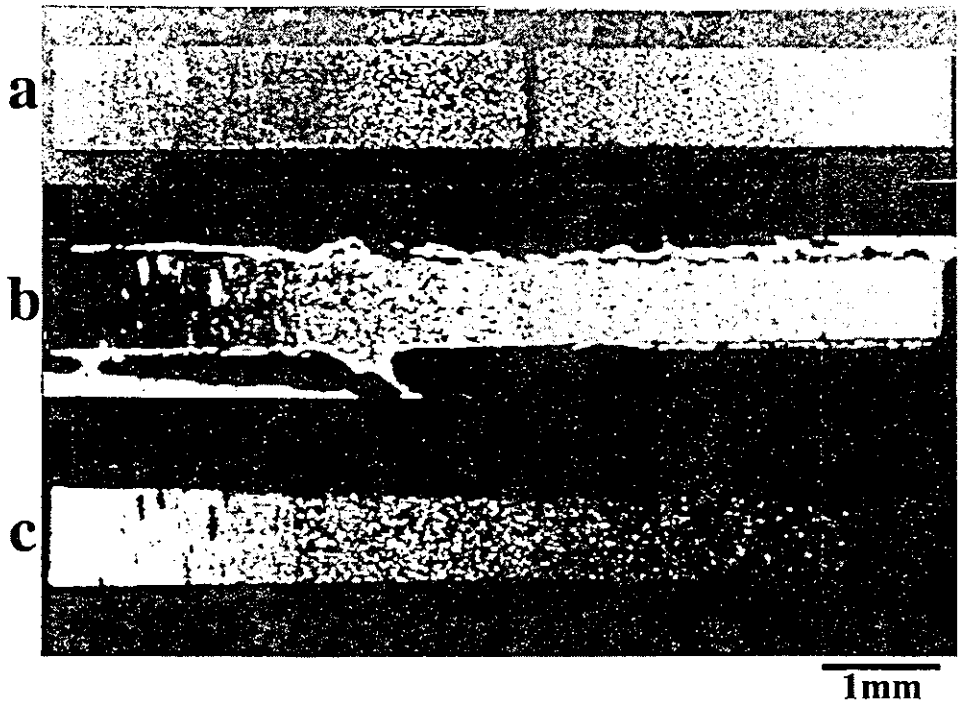

Fig. 12. Ti/HAP FGM implant made by SPS after three point flexural test (a) and Ca (b), Ti (c) mappings by EPMA after 8 week insertion in bone marrow of femora of rat.

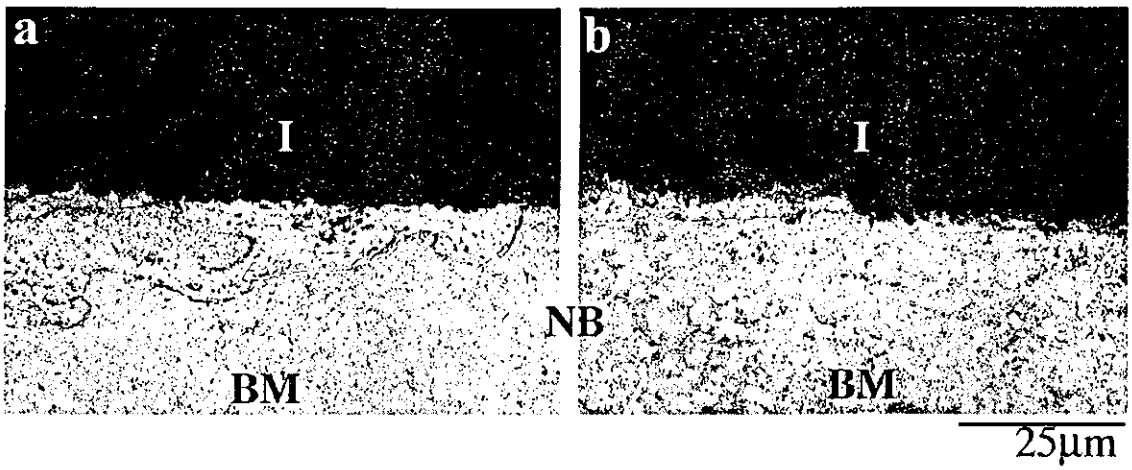

Fig. 13. Histological image around the Ti side (a) and the HAP-rich side (b) in the Ti/HAP FGM implant inserted in femora of rat for 16 weeks. I: implant, NB: new bone, BM: bone marrow.

For the observation of new bone formation around the implant which was inserted in the femora of rats, the compositional image by reflection electrons [1,11,30] and elemental mapping by EPMA and XSAM [11–13,20–22] were applied as well as the conventional method to observe histologically the stained thin specimen by optical microscopy. The contrast of those imaging methods is based on the electronic structure of specimens. Specimen preparation is simple without the ultra thin sectioning and staining. The recognition and evaluation of new bone area is easy. The light microscopic image of the stained tissue obtained by conventional means presents some ambiguity in tissue interpretation, depending on the degree of staining. Therefore, the substantial experience is necessary for proper interpretation of the observed features. On the other hand, the bone region is unambiguously evident in the Ca mapping, providing a basis for clear interpretation. The mapping method also can provide the distribution of each component element.

The difference in the distribution density of component atoms and of the resulting ratio of one element to

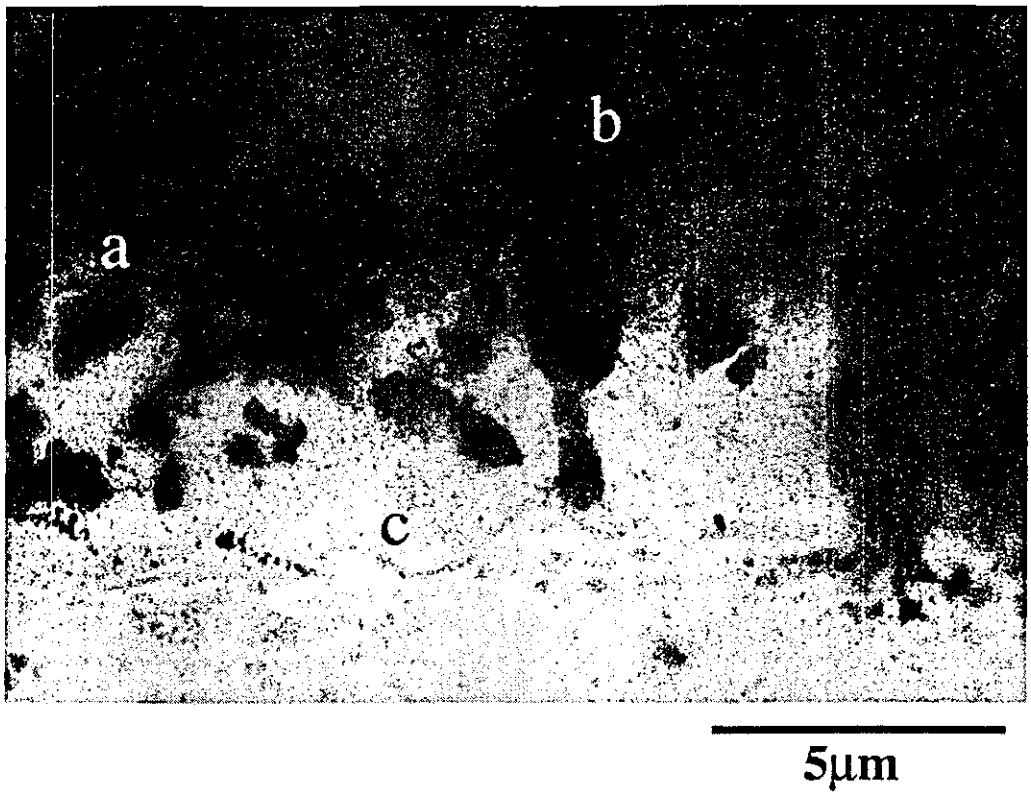

Fig. 14. Enlargement of new bone formation around HAP rich region of Ti/HAP FGM: a: HAP matrix, b: Ti particles, c: new bone.

another also can be obtained. In bone formation and apatite ceramics, the ratio of Ca/P in a wide range of non-stoichiometric compositions is often of major interest. It is possible to obtain such elemental ratio using the elemental analysis and mapping method. The typical example is found in Fig. 3 where dephospored region was visualized. XSAM was more sensitive to the heavier elements such as Ni and Co [21] shown in Figs. 8 and 12, although the spatial resolution was 100 μm or 10 μm, much lower than 1 μm in EPMA. On the other hand, the different tissues can be distinguished by the usual histopathological method which uses staining and light microscopic observation. Therefore the combination of histological observation and elemental mapping techniques could lead to the clear interpretation of the observed microstructural tissue, together with the additional information about the components.

4.3. Mechanical properties

The measurement of the properties of the uniform Ti–HAP specimens made by SPS showed that the density is very close to the true density, and the fracture toughness increases remarkably with the addition of Ti from 0.7 MPa·m$^{1/2}$ of pure HAP to 3.8 MPa·m$^{1/2}$ of Ti–50 vol.% HAP [19]. The addition of Ti to HAP had much effect on the increase of fracture toughness and other mechanical properties. Compression strength of bone is approximately 150 MPa. The Ti/20HAP FGM has approximately the comparable strength.

For Ti/100HAP FGM decomposition effect in sintering process is not negligible. Internal stress also arises from the difference of sintering shrinkage and thermal expansion coefficient at the interface from one region to others. To avoid autodestruction sintering temperature was lowered by use of SPS. There was much improvement in sintering by SPS compared with the conventional CIP and furnace sintering method. SEM observation showed that SPS can enhance the sintering effect in spite of the lower sintering temperature.

It is, however, still the compromised condition and sintering is imperfect. Ti–HAP composite is in a first approximation the physical mixture of both particles and there is no binding force between Ti and HAP particles. The strength of 60–90HAP region is not sufficient. Fracture of FGM occurs near the weakest region or its neighbor. In the three point flexural test of Ti/HAP FGM prepared with the SPS pressure 40 MPa, fracture occurred, deviated from center, in the HAP-rich side which is weaker. In the FGM prepared with 80 MPa, fracture occurred inside the single layer in the center. The flexural strength was increased to 36 MPa and the compressive strength 88 MPa, respectively.

The strength obtained here is not enough for practical use at moment. One of the reasons other than decomposition problem is the widest composition gradient

from 0 to 100% HAP, which is the most difficult to attain the perfect properties. If the range of gradient is limited up to 40% as shown in Fig. 7, it has enough strength durable to the clinical practice.

The decreasing tendency of hardness to the direction of tooth root region in Fig. 5b would contribute to the stress relaxation, which would relieve jaw bone from damage by imposition of high spike of impact stress on implant.

4.4. Biocompatibility

HAP is the main component of hard tissue such as bone and teeth. Ti is one of the best biocompatible metals and is commonly used for implant. Co is an important alloying element in non-precious dental alloys. Co–Cr is used for denture and orthodontic wire. Nickel, one of the major alloying elements for industrial materials such as stainless and Ni–Cr, is a typical element to evoke an allergic reaction. Ni–Cr alloy, which used to be a popular dental material, is now decreased in its usage in dentistry. Ni as an alloying element is mostly substituted by Co. Ni–Ti is used as orthodontic wire for initial treatment of leveling the irregular teeth row, utilizing its superelasticity as one variant phenomenon of shape memory effect. Ag is an important alloying elements of dental alloys. It is also often used as anti-bacterial materials. These materials as well as other refractory metals were used for implantation and compared to see the effect on tissue response.

No inflammation was observed for Ti implant inserted in soft tissue after one week. The histological observation of stained specimen by optical microscopy showed that the thin fibrous connective tissue was formed uniformly, surrounding an implant with constant thickness. Refractory metals of Ti, Zr, Hf, Nb, Ta except V in the IVa and Va groups, Re in the VIIIa group [1], Ti (N) [31,32] and TiN showed very little inflammatory reaction in animal experiments both in hard tissue and in soft tissue. Dissolution of these elements into tissue was not observed by elemental mapping. They have sufficient biocompatibility with a slight difference in new bone formation around implant in hard tissue.

Ni, implanted in soft tissue, induced severe inflammation [20]. The inflammatory area was coincided with the dissolved region of Ni revealed by Ni mapping of XSAM as seen in Fig. 8. There was relation between the gradient concentration of dissolved Ni and the degree of degeneration in soft tissue as a function of distance from Ni implant surface.

Although Fe was dissolved most of all metals tested in the present paper with the difference of more than one order, tissue did not suffer the serious inflammation (Fig. 9). The formation of fibrous connective tissue surrounding implant was observed in the early stage in Fe, while slightly delayed in Ag and stainless steel (SUS316), which reflects the difference of biocompatibility sensitively.

In the case of the implantation test of Ti/Co FGM [16] into soft tissue (Fig. 10), the thin fibrous connective tissue with the thickness of a few layers of fibroblast was formed at the side of pure Ti. The tissue layer thickness increased gradually with the Co concentration, forming more inflammatory tissue in the Co rich region, although tissue was not so severely deteriorated in Co as in Ni. The dissolved region of Co revealed by XSAM mapping and the inflammatory tissue region were in accordance with each other. The change of concentration of Co affected on the biocompatibility, which caused the change of tissue response. In Ti|V biimplant inserted in the tibia of rabit the new bone formation was severely depressed in the V side.

Co caused inflammatory change, while Ni exhibited severe degeneration and necrosis. In both elements the dissolved region and the inflammatory tissue region were corresponded each other. The tissue reacted gradiently in response to the gradient composition of FGM materials. Epple et al. used the Ni/Ti FGM to evaluate the cytotoxicity for different composition with a single specimen [33]. Their in vitro test also showed the gradient cell reaction.

The difference in bioreaction was relatively easy to recognize for the combination of biocompatible and biomalignant materials as in the case of Ti/Co FGM implant in soft tissue and Ti|V biimplant in hard tissue. It was difficult, however, to show the difference for the combination of biocompatible materials. In the implantation test of Ti/20HAP FGM into hard tissue there was only minor difference in new bone formation between the pure Ti region and the HAP-rich region. This is primarily because both Ti and HAP have good biocompatibility. In such a case the influence of other factors are often dominant. The new bone formation is easily affected by the shape, porosity, surface roughness of implants, the inserted position, distance from cortical bone and perforated region, and individual difference of animals other than implant materials.

It was shown that the coexistence of the HAP component seemed to induce the effect to accelerate the formation of new bone from the earlier stage under the ideal experimental conditions for Ti/100HAP. Fig. 14 showed that the maturation of new bone preceded in the HAP-rich region. This effect worked gradiently to the graded composition of Ti/HAP FGM implant.

The both gradient reactions to FGM, formation of fibrous connective tissue in soft tissue and osteogenesis in hard tissue, imply thus the possibility to control the tissue response over mm to μm scales in each part through the designed gradient composition and structure of FGM implant. This would contribute to the application of biomaterials for use as artificial internal organs.

Brinell hardness of Ti/HAP FGM decreased from 61 in pure Ti to 15 in pure HAP as shown in Fig. 5b. Although the hardness in HAP region is not sufficient for practical use, the decreasing tendency of hardness toward the tooth root contributes to stress relaxation in the implanted region of bone.

The gradient functions in both the biochemical affinity to osteogenesis and the mechanical properties with stress relaxation effect could contribute to the efficient biocompatibility. We may also include other functions for functionally graded implant such as abrasion resistance which is important in the artificial joint and abutment part in dental implant [31,32] to avoid the cytotoxicity by minute particles, originated from their size effect [34,35].

5. Conclusions

1. Ti/HAP and other FGM specimens were fabricated by powder metallurgy to optimize both mechanical properties and biocompatibilities.
2. Electric furnace heating, high frequency induction heating and spark plasma sintering (SPS) methods were used for sintering and compared. The stable Ti/HAP FGM implant could be successfully fabricated by application of SPS.
3. Ti/HAP showed that the maturation of newly formed bone was preceded in the HAP rich region.
4. The gradient functions in both the biochemical affinity to osteogenesis and the mechanical properties with stress relaxation in Ti/HAP FGM could attain the efficient biocompatibility for implant.
5. The study demonstrated that the tissue reaction changes gradiently in response to the gradient composition or structure of materials. This implies the possibility to control the tissue response by functionally graded structure of biomaterials.

Acknowledgements

Research was performed under Grant-in-Aid for Scientific Research (B)(2) from the Ministry of Education, Science, Sports and Culture of Japan, and Health and Laybour Sciences Research Grants in Research on Advanced Medical Technology from the Ministry of Health, Laybour and Welfare of Japan. The authors are grateful to Dr. Koichi Omamyuda of Sumitomo Osaka Cement for the supply of HAP.

References

[1] Matsuno H, Yokoyama A, Watari F, Uo M, Kawasaki T. Biocompatibility and osteogenesis of refractory metal implants, titanium, hafnium, niobium, tantalum and rhenium. Biomaterials 2001;22:1253–62.
[2] Driessens FCM, Verbeeck RMH. Biominerals. Boca Raton: CRC Press; 1990.
[3] Aoki H. Science and medical application of hydroxyapatite. Tokyo: Japanese Association of Apatite Science; 1991.
[4] Aoki H. Medical applications of hydroxyapatite. Tokyo: Ishiyaku EuroAmerica; 1994.
[5] Uo M, Mizuno M, Kuboki Y, Makishima A, Watari F. Properties and cytotoxicity of water soluble Na..O-CaO-P..O.. glasses. Biomaterials 1998;19:2277–84.
[6] Imai T, Watari F, Yamagata S, Kobayashi M, Nagayama K, Nakamura S. Mechanical properties and estheticity of FRP orthodontic wire fabricated by hot drawing. Biomaterial 1998; 19(23):2195–200.
[7] Watari F, Yamagata S, Imai T, Nakamura S, Kobayashi M. The fabrication and properties of aesthetic FRP wires for use in orthodontics. J Materials Science 1998;33:5661–4.
[8] Hirai T. Functionally gradient materials. In: Cahn RW, Haasen P, Kramer EJ, editors. Materials science and technology, vol. 17B: processing of ceramics part 2. Weinheim: Verlagsgesellschaft; 1996. p. 293–341.
[9] Takahashi H, Watari F, Nishimura F, Nakamura H. Functionally gradient materials of titanium-apatite and titanium-silica for dental use. J Jap Soc Dental Mater Devices 1992;11(3):462–8 [in Japanese].
[10] Watari F, Yokoyama A, Saso F, Uo M, Kawasaki T. Functionally gradient dental implant composed of titanium and hydroxyapatite. In: Ilschner B, Cherradi N, editors. Proc. 3rd Int. Symp. Structural & Functional Gradient Materials. Lausanne: Polytech. Univ. Romand; 1995. p. 703–8.
[11] Watari F, Yokoyama A, Saso F, Uo M, Kawasaki T. Elemental mapping of functionally graded dental implant in biocompatibility test. In: Shiota I, Miyamoto Y, editors. Functionally graded materials 1996. Amsterdam: Elsevier; 1997. p. 749–54.
[12] Watari F, Yokoyama A, Saso F, Uo M, Kawasaki T. Fabrication and properties of functionally graded dental implant. Composites Part B 1997;28B:5–11.
[13] Watari F, Yokoyama A, Saso F, Uo M, Matsuno H, Kawasaki T. Imaging of gradient structure of titanium/apatite functionally graded dental implant. J Jpn Inst Metals 1998;62(11):1095–101 (in Japanese).
[14] Watari F, Yokoyama A, Saso F, Uo M, Matsuno H, Kawasaki T. Biocompatibility of titanium/hydroxyapatite and titanium/cobalt functionally graded implants. In: Kayser WA, editor. Functionally Graded Materials 1998. Zurich: Trans Tech Publications; 1999. p. 356–61.
[15] Watari F, Yokoyama A, Saso F, Matsuno H, Uo M, Kawasaki T. Biocompatibility and bioreactivity of Ti-based functionally graded implant. In: Vincenzini P, editor. Advances in science and technology (Proc. 9th CIMTEC-World Forum on New Materials), vol. 28. Materials in clinical applications. Faenza: Techna Srl; 1999. p. 245–50.
[16] Watari F, Yokoyama A, Matsuno H, Miyao R, Uo M, Tamura Y, Kawasaki T, Omori M, Hirai T. Gradient tissue reaction induced by functionally graded implant. In: Trumble K, Bowman K, Reimanis I, Sampath S, editors. Functionally graded materials 2000, ceramic transaction 114. Am. Ceramic Soc; 2001. p. 73–80.
[17] Watari F, Yokoyama A, Matsuno H, Miyao R, Uo M, Kawasaki T, Omori M, Hirai T. Fabrication of functionally graded implant and its biocompatibility. In: Ichikawa K, editor. Functionally graded materials in the 21st century: a workshop on trends and forecasts. Boston: Kluwer Academic; 2001. p. 187–90.

[18] Watari F, Kondo H, Miyao R, Omori M, Okubo A, Hirai T, Yokoyama A, Uo M, Tamura Y, Kawasaki T. Effect of spark plasma sintering pressure on the properties of functionally graded implant and its biocompatibility. J Jpn Soc Powder Powder Metallurgy 2002;49(12):1063–9 [in Japanese].

[19] Yokoyama A, Watari F, Miyao R, Matsuno H, Uo M, Kawasaki T, Kohgo T, Omori M, Hirai T. Mechanical properties and biocompatibility of titanium-hydroxyapatite implant material prepared by spark plasma sintering method. In: Proc. 13th Int. Symp. Ceramics in Medicine, Bologna, Italy, 22–26 Nov. 2000. Key Engineering Materials vols. 192–195, 2001. p. 445–8.

[20] Uo M, Watari F, Yokoyama A, Matsuno H, Kawasaki T. Dissolution of nickel and tissue response observed by X-ray analytical microscopy. Biomaterials 1999;20(8):747–55.

[21] Uo M, Watari F, Yokoyama A, Matsuno H, Kawasaki T. Visualization and detectability of rarely contained elements in soft tissue by X-ray scanning analytical microscopy and electron probe micro analysis. Biomaterials 2001;22:1787–94.

[22] Uo M, Watari F, Yokoyama A, Matsuno H, Kawasaki T. Tissue reaction around metal implants observed by X-ray scanning analytical microscopy. Biomaterials 2001;21:677–85.

[23] Matsuo S, Watari F, Ohata N. Fabrication of functionally graded dental composite resin post and core by laser lithography and finite element analysis of its stress relaxation effect on tooth root. Dental Mater J 2001;20(4):257–74.

[24] Satoh N, Ueda Y, Yorimoto T, Aida H, Matsuo S, Ohata N, Watari F. Firing shrinkage of porcelain-resin composites prepared by laser lithography. Dental Mater J 1999;18(4):444–52.

[25] Konishi J, Watari F, Kawamoto C, Sano H. Effect of sphericalyzed particles on the firing contraction of porcelain inlay processed by cold isostatic pressing. J Biomed Mater Res 2003;66B:553–8.

[26] Watari F, Cowley JM. The study of oxide formation on (001), (011), (111) and (113) surfaces of Cr thin films using STEM-microdiffraction methods. Surface Science 1981;105:240–64.

[27] Watari F, Delavignette P, Van Lunduyt J, Amelinckx S. Electron microscopic study of dehydration transformations III: high resolution observation of reaction process: FeOOH..Fe2O3. J Solid State Chemistry 1983;48:49–64.

[28] Kobayashi Y, Ohshima Y, Ikeda T, Komatsu H, Watari F, Shimokobe H. AFM and SEM observation of morphological changes of human dentin surface by treatment of acidic agents. Dentistry in Japan 1995;32:46–51.

[29] Watari F. In situ etching observation of human teeth in acid agent by atomic force microscopy. J Electron Microscopy 1999; 48(5):537–44.

[30] Watari F. Compositional and morphological imaging of laser irradiated human teeth by low vacuum SEM, confocal laser scanning microscopy and atomic force microscopy. J Mater Sci Med 2001;12:189–94.

[31] Tamura Y, Yokoyama A, Watari F, Uo M, Kawasaki T. Mechanical properties of surface-nitrided titanium for abrasion resistant implant materials. Materials Transactions 2002;43(12): 3043–51.

[32] Tamura Y, Yokoyama A, Watari F, Kawasaki T. Surface properties and biocompatibility of nitrided titanium for abrasion resistant implant materials. Dental Mater J 2002;21(4):355–72.

[33] Bogdansky D, Kller M, Mller D, Muhr G, Bram M, Buchkremer HP, Stver D, Choi Jongsik, Epple M. Easy assessment of the biocompatibility of Ni-Ti alloys by in vitro cell culture experiments on a functionally graded Ni-NiTi-Ti material. Biomaterials 2002;23:4549–55.

[34] Kumazawa R, Watari F, Takashi N, Tanimura Y, Uo M, Totsuka Y. Effects of Ti ions and particles on cellular function and morphology of neutrophils. Biomaterials 2002;23:3757–64.

[35] Tamura K, Takashi N, Kumazawa R, Watari F, Totsuka Y. Effects of particle size on cell function and morphology in titanium and nickel. Materials Transactions 2002;43(12): 3052–7.

Key Engineering Materials Vols. 254-256(2004) pp. 919-922
online at http://www.scientific.net

Effects of Micro/Nano Particle Size on Cell Function and Morphology

K. Tamura[1], N. Takashi[1], T. Akasaka[2], I. D. Roska[2], M. Uo[2],
Y. Totsuka[1], F. Watari[2]

[1] Department of Oral and Maxillofacial Surgery, Graduate School of Dental Medicine,
tam@den.hokudai.ac.jp
[2] Dental Materials and Engineering, Graduate School of Dental Medicine,
Hokkaido University, kita 13 nishi 8, kita-ku, Sapporo, 060-8586, Japan

Keywords: particle, biomaterial, titanium, titanium dioxide, carbon nanotube, biocompatibility

Abstract. The cytotoxicity of micro/nano particles in Ti, TiO and carbon nanotube was investigated by in vitro biochemical analyses using human neutrophils. The particles smaller and larger than the neutrophils were used to determine the relationship between cell and particle size with respect to cytotoxicity. As the particle size decreased, the cell survival rate was decreased and, with the good corresponding relation to this, the value of lactate dehydrogenase (LDH), which is the indication of cell disruption, was increased. The release of superoxide anion showed the increasing tendency. Proinflammatory cytokines were detected distinctly for 3μm or smaller particles and very little in more than 10μm, which is closely related to the phagocytosis by neutrophils. ICP elemental analysis showed that the dissolution from Ti particles was below detection limit. Micro and nano particles stimulated the cell reactions according to the results of the human neutrophil functional tests. As the particle size was smaller, the inflammation was pronounced. The fine particles less than 3μm caused distinctly the inflammation in the surrounding tissue. All these results indicated that the cytotoxicity was induced due to the physical size effect of particles, which is different from the ionic dissolution effect. The clinical phenomenon confirmed the result obtained in vitro cell tests. The neutrophils stimulated by fine particles may cause the inflammatory cascade and harm the surrounding tissue.

Introduction

Ti and its alloys are the commonly used material in plastic surgery because it is one of the most biocompatible metals [1,2]. Ti is highly corrosion-resistant at ambient temperature due to its thin and stable protective oxide layer formed on its surface. In this sense Ti is the ideal metallic material for implant [3,4]. However, it is clinically reported that the abraded fine titanium particles produced in sliding parts of artificial joints often caused inflammation in the surrounding tissue [1,2]. However, little is known about the effect of micro/nano particles on cellular function and the relevance between *in vivo* and *in vitro* findings. The purpose of this study is to analyze the vital reactions of human neutrophils to the Ti, TiO_2 particles and carbon nanotubes and their size effect.

Materials and probe cells

The dependence of cytotoxicity on particles size in titanium, titanium oxide (TiO_2) and carbon nanotubes was investigated by biochemical functional analysis and by microscopic observation of cellular morphology.

Particles. The Ti, TiO_2 and carbon nanotubes particles colloid solutions were prepared. ICP elemental analysis showed that the dissolution from Ti particles were below detection limit. The carbon nano-tubes is 99% purity. The solubilization distributed processing was carried. The average diameter and size distribution of the TiO_2 particles and carbon nanotubes were determined by electron microscopy (SEM) and by laser scattering particle distribution analyzer (SALD-7000, Shimadzu).

The various sizes of Ti, TiO_2 and carbon nanotubes particles were mixed with HBSS (Hanks' balanced salt solution). The colloid solutions were adjusted to PH 6.8 by 1N NaOH solution, sterilized by autoclave and dispersed by sonicator [5,7].

Cells. Human peripheral blood was obtained from healthy volunteers in our group. Neutrophils were separated from the blood using the 6% isotonic sodium chloride containing the hydroxyethyl starch and lymphocyte isolation solution (Ficoll-Hypaque)[6,7]. The cells were maintained in HBSS. After particles were kept dispersed, neutrophils were added, and incubated in a humidified atmosphere of 5% carbon dioxide at 37 °C for 60 minutes. The experiments were performed using cells within 3 hours after collection of blood and the cell density was adjusted to 10^6 cells / ml [7].

Methods

Cell survival rate, leakage of lactate dehydrogenase (LDH), product of superoxide anion, and release of cytokines of tumor necrosis factor-alpha (TNF-alpha), interleukine-1 beta (IL-1beta) were measured to analyze biochemical reaction.

(1) Cell survival rate: The cell stained with trypan blue population was counted under an optical microscope using Thomas' hemacytometer. The number of vital cell in the control specimen was considered as 100%.

(2) LDH activity: The LDH values of samples were measured using the lactate dehydrogenase C test kit (Wako Pure Chemical Industries) and by spectrophotometry.

(3) Superoxide anion production: Superoxide anion (O_2^-) was assayed by measuring the superoxide dismutase-inhibiting reduction of equine ferricytochrome C (550 nm). The reaction was promoted by adding 1.39mM PMA (phorbol 12-myristate 13-acetate) [7].

(4) Cytokine release: TNF-alpha and IL-1 beta in the supernatant was measured using ELISA kits (Endogen) [7].

The values are expressed as means +/- standard deviation (n=6). Data were analyzed by Student's-t test with the level of significance set at 5%.

The pathological and morphological changes were observed by optical microscopy and SEM.

Results

Ti particles diameter were 3, 10, 50, and 150 μm and TiO_2 particles were 0.05, 0.5, and 3 μm in average size, as confirmed by SEM and the particle distribution analyzer. The SEM image shows carbon nanotubes with diameter of 20 nm and length of 100 nm.

The significant difference of the survival rate from control was observed in all nano particles (Fig.1). The Ti micro particles showed clearly the size dependency. The cell survival rate decreased, when the particle size became smaller. The nanoparticle of TiO_2 also showed the similar tendency. The lowest mean value of the survival rate was 84.6% in the size 50 nm for TiO_2 particles, which were the smallest particles in this study.

LDH showed the tendency to increase as the particle size became smaller (Fig.2). The LDH level of 147.2 Wroblewski unit was significantly higher in the 50 nm than the other larger sizes.

The neutrophils stimulated by the 3 μm or less particles showed the large productions of superoxide anion. The other larger size particles were slightly higher than control solutions (Fig.3).

There is a clear difference in the emission of inflammatory cytokines for 3 μm and 10 μm (Fig.4). The distinct release of TNF- alpha was observed in 3 μm or less particles. There was no statistical difference of cytokines under 3 μm. The IL-1beta showed the similar

SEM observation revealed the degenerative changes in the morphology of neutrophils (Fig.5). The activated neutrophils extended some pseudopods and phagocytized particles into the cytoplasm. 50nm TiO_2 particles and carbon nanotube induced the morphological change of neutrophils. After 6 hours, the atrophied and destroyed neutrophils were observed.

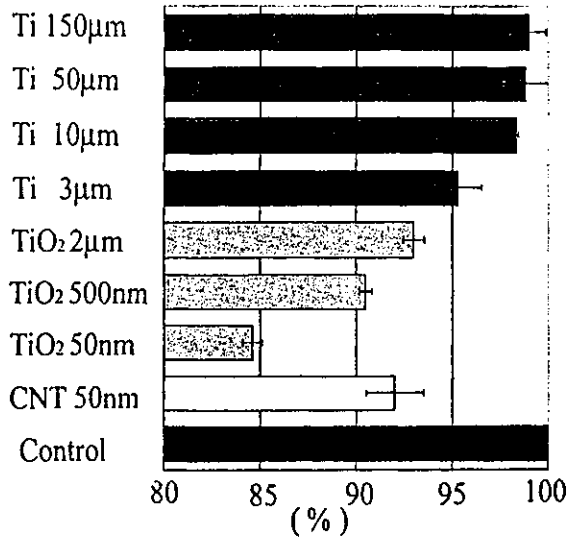

Fig.1 Cell survival rate

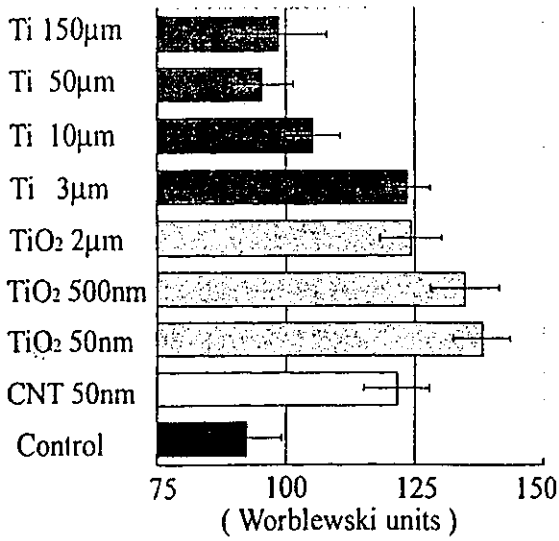

Fig.2 LDH activity

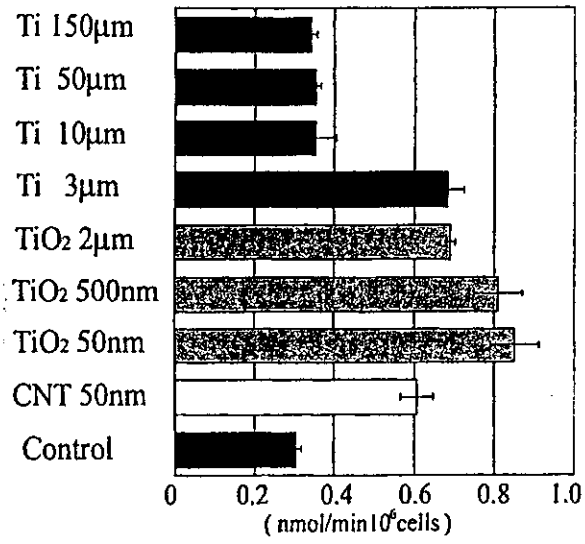

Fig.3 Supcroxide anion

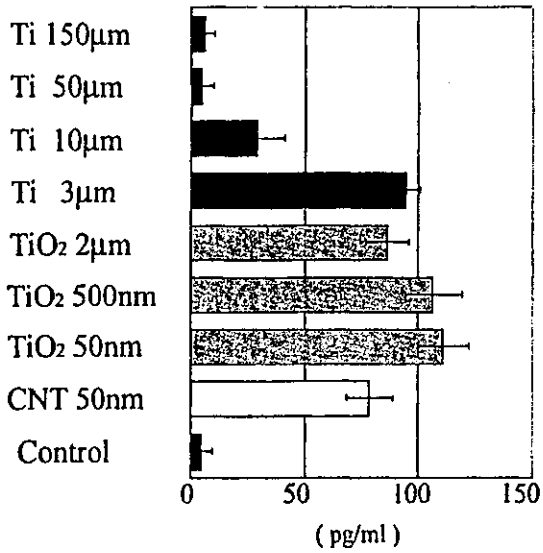

Fig.4 TNF-alpha